Two-dimensional Fourier transform ESR in the slow-motional and rigid limits: SECSY-ESR ☆

Baldev R. Patyal, Richard H. Crepeau, Dan Gamliel and Jack H. Freed
Baker Laboratory of Chemistry, Cornell University, Ithaca, NY 14853-1301, USA

Received 9 August 1990

Two-dimensional Fourier transform ESR has now been extended to the slow-motional and rigid limit regimes which require spectral bandwidths of 200–250 MHz and sub-nanosecond time resolution in echo decays. Two-pulse SECSY-ESR on nitroxides is shown to provide detailed structural information from the effects of nuclear modulation and slow-motional information from both the main ESR spectrum as well as the nuclear modulation.

1. Introduction

An important recent development in ESR has been two-dimensional Fourier transform ESR (2D-FT-ESR) [1–8]. It has been applied primarily to motionally narrowed spectra, e.g. for nitroxides with a spectral width of about 100 MHz. The particular variant that has proved most useful up to now has been 2D-FT-ELDOR (electron–electron double resonance), which has been shown to be an effective method to quantitatively measure magnetization transfer by the spin-relaxation processes of Heisenberg spin exchange, and nuclear spin-flip transitions induced by intramolecular electron–nuclear dipolar interactions.

Earlier work, prior to the development of FT-ESR methods, showed that 2D-ESR could be performed by field-swept electron-spin-echo (ESE) methods for ESR spectra in the slow-motional regime [5–7, 9–11]. In these experiments, in contrast to FT methods wherein a non-selective pulse is utilized to irradiate the whole spectrum, one uses a "soft-pulse" that irradiates only a very small region of the spectrum. Thus it is necessary to repeat this experiment many times as one sweeps the magnetic field through the spectrum. Nevertheless, these methods were shown to be very useful because they provide the important spin-relaxation information across the otherwise broad inhomogeneous rigid-limit-like spectrum. In particular, the two-pulse field-swept 2D-ESE experiment provides the homogeneous line shapes in the second dimension as a function of ESR spectral position, from which the homogeneous T_2 can be determined as a function of ESR spectral position. Since it is the homogeneous T_2 that is sensitive to the motional dynamics, this enhanced resolution means that slower motions than can be studied by cw-ESR are possible to study in great detail by 2D-ESE. The "T_2 plots" obtained in a variety of studies were found to be very sensitive not only to motion in the region $10^{-6} < \tau_R < 10^{-3}$ s but also to the motional models used to describe rotational reorientation [5,6,9–11].

The 2D-ESE field-swept technique would, in principle, be amenable to the newer 2D-FT-ESR methods, which have the advantage of (a) greatly reduced data acquisition times, because the whole spectrum is irradiated simultaneously; and of (b) $\pi/2$ pulse widths significantly shorter (e.g. 5 ns) than the relevant T_2's, which both reduce dead time and any spectral distortions arising from the use of very long (e.g. 80 ns) selective $\pi/2$ pulses in the field-swept method. Another advantage relates to the so-called "nuclear modulation", which leads to electron-spin echo envelope modulation (ESEEM) in conventional ESE experiments in the rigid limit [12–

☆ Supported by NSF Grant CHE 9004552 and NIH Grant GM25862.

14]. In a recent theoretical study, it was shown that 2D-FT-ESR methods would provide greater resolution of the spectral effects of nuclear modulation and would thereby provide more detailed structural information than the corresponding ESEEM spectra [15]. Furthermore, in order to perform accurate studies on nuclear modulation, it is necessary to irradiate the allowed and forbidden ESR transitions simultaneously. This is consistent with the requirements of non-selective pulses in FT-ESR rather than the weak pulse requirement in the field swept methods, especially for such nuclei as protons. Studies of the nuclear modulation are important not only for structural information. Rotational motions significantly affect the nuclear modulation and thereby provide another means to study such motions [5,6].

However, 2D-FT-ESR in the slow motional regime poses several challenges beyond those for the fast motional regime. First of all, one must irradiate spectra of 200–250 MHz extent, requiring (a) greater microwave magnetic fields for the pulses to cover the whole spectrum, yet (b) the resonator must have lower Q in order not to filter out higher-frequency spectral components. Conditions (a) and (b) are conflicting and require special optimization of the resonator. Secondly, the free induction decay (FID) is extremely rapid. Thus, it will be entirely lost in the spectrometer dead-time $\tau_d \approx 100$ ns. Instead, one collects the spin echo decay at a time $\tau_1 > \tau_d$ after the echo-forming pulse, since the echo decay is nearly equivalent to the FID. But a rapid echo decay requires very short (at least nanosecond) time resolution, as well as substantial signal-to-noise to permit detection of the echo decay over reasonable time intervals t_2 (of order of at least 50–100 ns).

It is now possible for us to satisfy these requirements and to perform 2D-FT-ESR in the slow-motional and rigid-limit regions for nitroxide samples. We report in this Letter our initial results with the two-pulse FT analogue of the older field-swept technique, which we call SECSY-ESR, and we indicate its potential for studies of molecular dynamics and structure.

2. Experimental

Our 2D-FT-ESR spectrometer has been described elsewhere [2,6]. Some modifications were necessary to ensure coverage of the spectrum over a bandwidth of 200–250 MHz and to enhance processing of weak signals. A high-power filter following the TWT with a bandpass extending from 9 to 9.6 GHz with 30 dB points at 8.8 and 9.8 GHz serves to reduce the white noise from the TWT outside our frequency range and to improve the dead time of the spectrometer. Following the limiter in the detection arm, a second microwave amplifier and attenuator combination (for a maximum combined gain of 80 dB) permits adjustment of the signal amplitude into the optimal range for data collection on the HP 54100A digitizing scope.

It is essential to use a low-Q high-filling factor resonator, and we have utilized a bridged loop gap resonator (BLGR) similar to that previously described [6,16], but with several improvements in order to enhance its structural stability when repeatedly cooled and heated and to permit accurate temperature control and coupling. By employing a cylindrical shield surrounding the BLGR we have obtained a slightly higher B_1 field at the sample, resulting in 200–250 MHz coverage from 5 ns 1 kW pulses. Coupling to the cavity is achieved with a single turn loop of wire perpendicular to the BLGR axis and capacitively coupled to the transmission line center conductor. Structurally, the adhesion of the silver paint to the glass cylinder making up the BLGR was enhanced by prior sandblasting of the glass with a fine CrO_2 powder to roughen the surface. The thickness of the silver paint on the BLGR and glass cylinder surrounding the resonator were adjusted to give the desired Q and the broad coverage required for the experiment.

All experiments were on ^{15}N-protonated tempone or ^{14}N perdeuterated tempone (PDT), 0.5 mM in 85% glycerol–15% H_2O and degassed to better than 10^{-6} Torr.

3. Results

3.1. Echo decays

We first consider the echo decay after the $\pi/2$–t_1–$\pi/2$–t_1–t_2 SECSY sequence, since its detection is at the heart of these experiments. An example of the

two quadrature components of the echo decay signal versus t_2 is shown in fig. 1 for the case of ^{14}N-PDT at $-83\,^{\circ}$C. One notes that it decays to the noise level within 50 ns. Fig. 1 shows the actual data points collected at 0.78 ns intervals as well as the smoothed curve obtained by applying linear prediction with singular value decomposition (LPSVD) simultaneously to the two quadrature signals [6]. The data were obtained by a special four-step phase cycle (cf. table 3, case (b) in ref. [15]) that cancels axial terms together with dc offsets (which would distort the echo decay), and at the same time the full effect of CYCLOPS is retained (which cancels "images" resulting from imperfections in the quadrature detector) [2,6]. Each step is averaged 64 times. Not shown in fig. 1 is the second pair of quadrature signals that is obtained by an additional four-step phase cycle, which differs from the first one in that the phase of the preparation pulse is advanced by $\pi/2$. These two complex signals, labelled S' and S'', respectively, constitute the full dual quadrature signal required in the 2D-FT experiment [1,2,6].

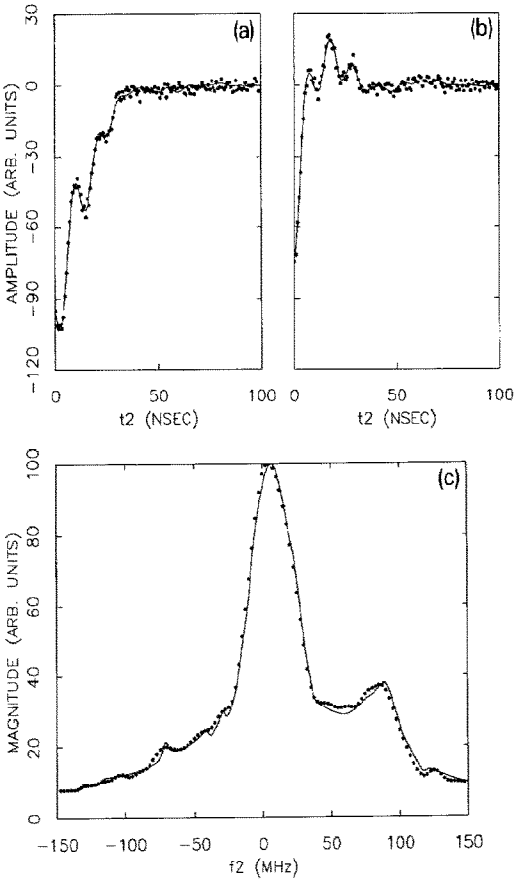

Fig. 1. Echo decay as a function of t_2 after the $\pi/2$–t_1–$\pi/2$–t_1–t_2 sequence for PDT at $-83\,^{\circ}$C, with $t_1 = 100$ ns. (a) and (b) show the two quadrature components. (●) actual data, smoothed curves obtained by applying LPSVD. (c) Magnitude Fourier transform spectrum of this echo decay. (●) points obtained by FFT of data shown in (a) and (b). Smoothed curve obtained by FFT of the LPSVD.

We present in table 1 the LPSVD results for the complex echo decay shown in fig. 1. This method removes much of the noise and represents the time series as a sum of decaying sinusoids to form

$$\sum_i A_i \cos(\omega_i t_2 + \phi_i) \exp(-t_2/T_{2,i}^{*}) .$$

As seen in fig. 1, it gives an accurate representation of the echo decay for the inhomogeneously broadened signal. Table 1 shows that there are only four principal components, and they have values of T_2^{*} mainly about 11–14 ns, but there are additional very weak components which are not unequivocally distinguishable as signal versus noise. The magnitude FFTs obtained from the original data and the LPSVD result are also shown in fig. 1. They further illustrate the sensitivity and resolution of these echo decays. Similar, though slightly improved resolution is observed at lower temperatures, whereas more broadened spectra with even shorter T_2^{*} are observed at higher temperatures (e.g. 9 ns at $-63\,^{\circ}$C) due to incipient motional effects. Most important is that we can reproduce fairly accurately the full 230 MHz spectrum with only small attenuation in the spectral wings. Also note that it is difficult to select the true "in-phase" or absorption component in f_2 for these

Table 1
Spectral components for echo decay from PDT at $-83\,^{\circ}$C, obtained by LPSVD along t_2

Amplitude (arb. units)	Frequency f_2 (MHz)	Decay constant T_2^{*} (ns)	Phase (deg)
14152	1.8	11	−170
3387	−21.9	12	−33
2669	88.0	14	−61
1194	23.3	27	−67
219	−71.0	40	92
179	116.5	42	168
112	−40.6	70	−115

broad inhomogeneous spectra especially given that there are significant phase variations across the 230 MHz spectrum due to the finite size of the B_1 field. (Typically we find 7–8° phase variation in 2.5 MHz variation of $\omega_2/2\pi$.) The quadrature components may be collected with arbitrary phase settings, and the 2D-LPSVD outlined below is employed whenever phase corrections are desired. Lastly, we note that ^{15}N-tempone has a spectral extent of about 200 MHz, and its echo decay followed by FFT shows even better coverage of the whole spectrum.

3.1. SECSY-ESR

In fig. 2 we show a series of SECSY-ESR spectra obtained at several temperatures for ^{15}N-tempone (and one temperature for ^{14}N-PDT). The spectra at −103°C are in the rigid limit. Each spectrum requires about an hour of data acquisition. One observes the principal ESR spectrum as a function of f_2 and centered along $f_1=0$ MHz (i.e. the 0 MHz slice). However, extending outward along f_1 are the proton (deuteron) modulation peaks. As the temperature is raised the central ESR spectrum as well as the modulation structure tends to broaden out due to the effects of increased rotational reorientation.

These 2D spectra were obtained from the full eight-step phase cycle providing S' and S'' as a function of t_1 and t_2. We used 128 steps of $\Delta t_1=10$ ns for PDT (and 5 ns for ^{15}N-tempone) starting from $t_{1,\min}=100$–130 ns to avoid dead-time distortions. It was shown [15] that the dual quadrature data are best represented in the form

$$S_{c-}=S'-\mathrm{i}S''\,. \tag{1}$$

This is the linear combination that provides just the spin echo data after phase cycling, and it would cancel out any residual FID-like contributions from the second pulse as well as related noise. Fig. 2 consists of the magnitude spectra from S_{c-}. The complex signals S' and S'' have been treated as follows. $S'(t_1, t_2)$ and $S''(t_1, t_2)$ are first fast-Fourier-transformed with respect to t_2 for each value of t_1 and then added according to eq. (1) to obtain $\hat{S}_{c-}(t_1, f_2)$. Then for each discrete value of f_2 from the FFT, an LPSVD is applied as a function of t_1 (after using simple smoothing procedures). The tables of decaying sinusoids obtained in this manner provide the 2D spectra in the form:

$$\hat{S}_{c-}(t_1, f_2) = \sum_n \sum_j C_{jn}(n\,\Delta f_2)\exp(-2m\,\Delta t_1/T_{2,jn}) \times \exp(\mathrm{i}\omega_{1,jn} m\,\Delta t_1+\phi_{1,jn})\,, \tag{2}$$

with $t_1=m\,\Delta t_1$ and $f_2=n\,\Delta f_2$. The weighting coefficient

$$C_{jn}=|C_{jn}(n\,\Delta f_2)|\exp(\mathrm{i}\phi_{2,jn})\,.$$

The LPSVD provides for each value of n the "amplitude" $|C_{jn}(n\,\Delta f_2)|$, frequency $\omega_{1,jn}$, damping $\frac{1}{2}T_{2,jn}$, and phase $\phi_{jn}\equiv(\phi_{1,jn}+\phi_{2,jn})$ for the j_nth decaying sinusoid. In general, the central spectrum as well as the stronger nuclear modulation peaks show up at nearly the same spectral positions within experimental error, i.e., $\omega_{1,jn}$ is (nearly) independent of n, but this need not be the case for $T_{2,jn}$. The phase $\phi_{2,jn}$ vary with n primarily due to the effects of finite B_1 (cf. above). This variation is found to be approximately independent of sinusoid j. Thus it is possible to reset the phases ϕ_{jn} to a common ϕ_2 and thereby to obtain the $\phi_{1,jn}$ from ϕ_{jn}. The phases $\phi_{1,jn}$, however, are affected by the finite dead time in t_1 and by the finite B_1. We find it most convenient to minimize the role of phases by plotting the magnitude spectra.

A typical set of LPSVD results for a constant f_2 slice is presented in table 2. One distinguishes the central line and the array of nuclear modulation peaks. The theory of 2D-ESR with nuclear modulation has been detailed elsewhere [15]. It is a generalization of the well-known theory for ESEEM [12–14]. Here we just write the expression for a single-proton case:

$$\begin{aligned} S_{c-}(t_1, t_2) &= \exp[-(2t_1+t_2)/T_2] \\ &\times\{k_+\cos(\omega_- t_2)+k_-\cos(\omega_+ t_2) \\ &+\tfrac{1}{4}k\{\cos(\omega_\alpha t_1+\omega_- t_2)+\cos(\omega_\beta t_1-\omega_- t_2) \\ &-\cos[\omega_-(2t_1+t_2)]+\cos(\omega_\alpha t_1+\omega_+ t_2) \\ &+\cos(\omega_\beta t_1+\omega_+ t_2)-\cos[\omega_+(2t_1+t_2)]\}\}\,, \end{aligned} \tag{3}$$

where

$$\omega_\alpha=[(\tfrac{1}{2}A+\omega_n)^2+(\tfrac{1}{2}B)^2]^{1/2}\,, \tag{4a}$$

$$\omega_\beta=[(\tfrac{1}{2}A-\omega_n)^2+(\tfrac{1}{2}B)^2]^{1/2}\,, \tag{4b}$$

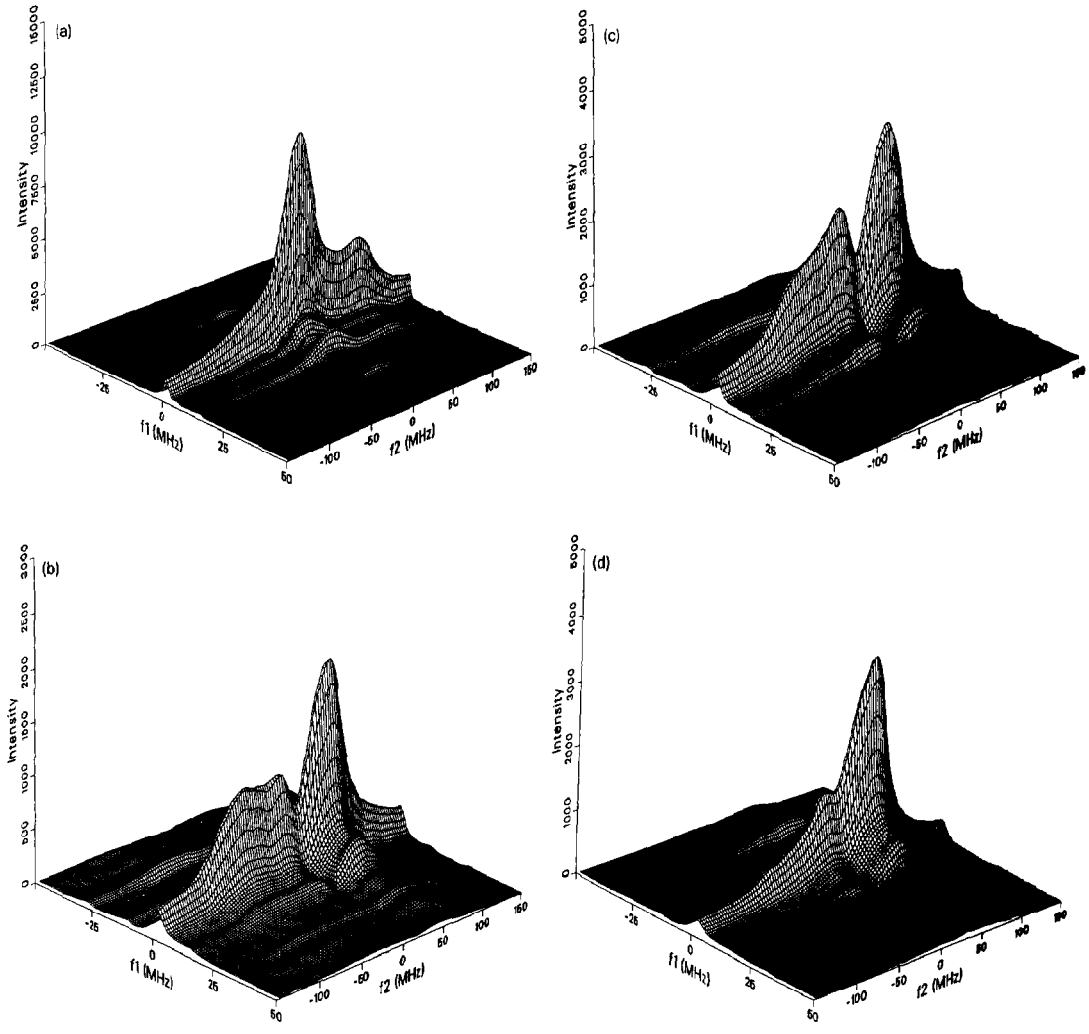

Fig. 2. Experimental SECSY-ESR spectra for (a) PDT at −103°C and for ^{15}N-tempone at the following temperatures: (b) −103°C, (c) −83°C, (d) −63°C. These spectra have been processed by LPSVD as described in the text in relation to eq. (2).

and

$$\omega_{\pm} = \tfrac{1}{2}(\omega_{\alpha} \pm \omega_{\beta}) , \tag{4c}$$

also

$$k = (\omega_n B_0/\omega_{\alpha}\omega_{\beta})^2 , \tag{5a}$$

and

$$k_{\pm} = \tfrac{1}{2}(1 - \tfrac{1}{2}k \pm \sqrt{1-k}) . \tag{5b}$$

Here ω_n is the proton Larmor frequency and A and B are, respectively, the secular and pseudosecular parts of the electron–proton dipolar interaction defined elsewhere [12], and they are a function of orientation. Thus the single-proton case will show modulation frequencies with respect to t_1 (or f_1) corresponding to $\pm\omega_{\alpha}$, $\pm\omega_{\beta}$, $\pm 2\omega_{-}$, and $\pm 2\omega_{+}$ (and they will depend also on t_2 (or f_2)). Additional protons (or deuterons) will lead to enhanced modulation peaks at these frequencies as well as "overtone" frequencies in analogy with ESEEM [12–14]. (Eq. (3) reduces to the standard ESEEM result by setting $t_2 = 0$ [12].) We find both theoretically and experimentally that the ^{14}N or ^{15}N nuclear modulation is negligible, because their $|\omega_n| \ll \frac{1}{2}A, \frac{1}{2}B$.

Table 2
Spectral components for SECSY experiment on ^{15}N-tempone at −83°C, obtained by LPSVD along t_1 [a]

Amplitude (arb. units)	Frequency f_1 (MHz)	Decay constant $\frac{1}{2}T_2$ (ns)	Phase (deg)
34748	0	211	−12
18394	0.15	288	135
8077	13.5	125	−126
2419	−12.3	142	41
934	−9.40	169	20
4336	21.0	32	43
646	9.38	300	−144
1341	−28.7	224	17
706	28.9	454	48
248	12.0	567	−126
1668	37.4	84	63
292	−16.0	227	−77
461	−36.2	234	−167
1419	51.3	41	−44
447	−42.7	129	−7

[a] This corresponds to the f_2=0 MHz slice that is shown in fig. 4.

The proton (deuteron) modulation is important, largely because there are several such nuclei present in tempone (or PDT) as well as in the solvent, and there is the additive effect noted above. The effects of these protons (deuterons) are best examined by simulations of the 2D-SECSY-ESR spectra. We show such simulations in fig. 3 for ^{15}N-tempone for three models: (i) a single ^{15}N nucleus and 12 completely equivalent methyl protons with hf tensors coincident with that of the ^{15}N nucleus; (ii) a single ^{15}N nucleus and 4 groups of 3 completely equivalent methyl protons geometrically displaced according to the known crystal structure [17] of tempone; (iii) the same as case (ii) but with a water molecule H-bonded to the N–O moiety. (In each case rapid internal rotation of the methyl groups is assumed.) The important observation is that the nuclear modulation along f_1 depends on spectral position given by f_2, and this variation with f_2 is distinctly different in the three cases. In fact, for the nitroxide spectrum the position f_2 provides a degree of orientational selectivity, and the effects of proton nuclear modulation are smeared out when we allow for a range of orientations of the protons in the molecule. A comparison of figs. 2 and 3 makes clear that our results are in better agreement with cases (ii) or (iii) with the former favored (perhaps implying solvent protons are not specifically H-bonded to the N–O moiety). Included in this observation is the fact that the main ESR spectrum along f_1=0 (0 MHz slice) is also dependent upon the precise model for the proton nuclear modulation. This can largely be attributed to the k_+ term in

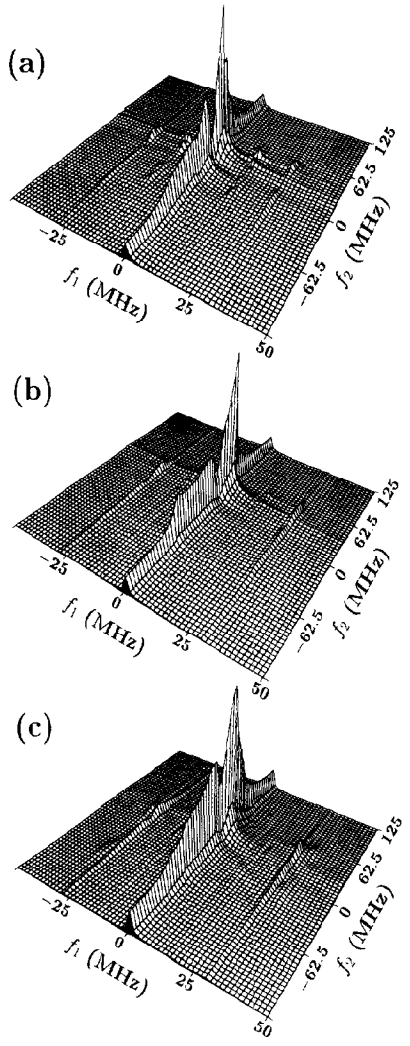

Fig. 3. Simulations of SECSY-ESR spectra in the rigid limit for ^{15}N-tempone for several models of the geometric arrangement of the protons: (a) 12 completely equivalent methyl protons; (b) four groups of three completely equivalent methyl protons (cf. text); (c) same as (b) but with an H-bonded water molecule. The methyl proton axial hf tensor used was $\bar{a}=-1.2$ MHz and $D=-6.2$ MHz, which for (b) and (c) had polar angles with respect to the ^{15}N hf tensor of $\theta=67°$ and the four values of $\phi=55°$, 125°, 235°, and 305°. For the two H-bonded water protons in (c) we used $\bar{a}=0$ with $D_1=20$ MHz, $\theta_1=180°$, $\phi_1=0$ and $D_2=9$ MHz, $\theta_2=140°$, $\phi_2=90°$.

eq. (3), which provides proton modulation on the main spectrum.

The rich information content of these SECSY-ESR spectra is best illustrated by examining slices versus f_1 for different values of f_2 at several temperatures. We show in fig. 4a the orientational (i.e. f_2) variation for PDT at $-103°C$ (rigid limit). One observes the deuterium modulation structure appearing at multiples of about ± 2 MHz, but there is also structure at about ± 14 and ± 28 MHz corresponding to solvent protons, which should be due to solvent H_2O near the nitroxide moiety. In fig. 4b the same slices are observed at $-63°C$, where there is appreciable motion. One observes that the central line as well as the modulation peaks are all broadened out by the motion, and there is reduced variation of the nuclear modulation across the spectrum. In fig. 4c the temperature variation of the central f_2 slice for PDT is illustrated. One sees that the deuteron structure smears out with an increase in the motional rate, but the proton structure seems less affected. This lower sensitivity of the proton structure to motion is illustrated in fig. 4d, which shows the temperature variation of the central f_2 slice for protonated ^{15}N-tempone. Whereas there is a broadening of the lines with increased motion, the proton structure retains its same basic pattern. This behavior is expected [5,18] because of the fact that rotational motion tends to average out the nuclear modulation when $\tau_R^{-1} \geqslant |A|, |B|$, so the smaller hf tensors for deuterons versus protons (by a factor of 6.54) are more affected by slower motions. The extensive lineshape changes of the deuteron modulation pattern and its variation with spectral position along f_2 should be very useful for detailed motional studies in conjunction with observations of the broadening of the central line.

We briefly mention two other observations. First of all, eq. (3) has terms in $\pm 2\omega_-$ which should appear very near to and overlapping with the principal spectral region, but it should be broader (due to the different orientations of the various protons), and it would be of opposite phase. Our SECSY-ESR results for protonated ^{15}N-tempone indeed show two components in the $f_1 = 0$ region (for $T \leqslant -80°C$) which are nearly opposite in phase (in the central region where S/N is best). However, for PDT we have not been able to distinguish two components by LPSVD; perhaps more extensive signal averaging would be

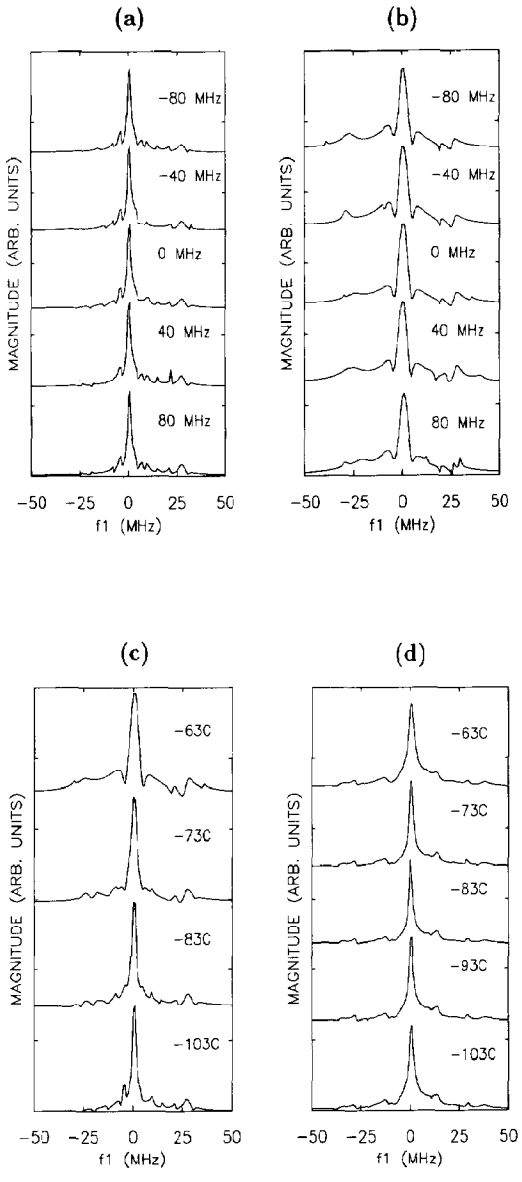

Fig. 4. Constant f_2 slices versus f_1 for SECSY spectra for PDT: (a) $-103°C$, (b) $-63°C$. Also the temperature variation of the central (0 MHz) f_2 slice for (c) PDT and (d) ^{15}N-tempone. For (c) T_2 is 266 ns ($-63°C$), 594 ns ($-73°C$), 1090 ns ($-83°C$), 1260 ns ($-103°C$). The τ_R values [9,10] for these four temperatures are respectively 17, 50–100, ≈ 500 μs and rigid limit (i.e. too slow to detect). These are results after processing by LPSVD. (Note that in this figure (unlike fig. 2) the SECSY spectra for the different temperatures have been adjusted to a common reference value of $f_2 = 0$ corresponding to the maximum in the ESR spectrum.)

required, since these components would be more nearly equal in frequency. However, the T_2's from the central ($f_1=0$) region are in good agreement with those previously obtained by Millhauser and Freed (MF) [9] and the τ_R values given in fig. 4, which are obtained from these T_2's, are in agreement with the previous work [9,10]. The 2D contours analogous to those given by MF can also be obtained from the LPSVD results for the central ($f_1=0$) region. We do not observe the significant T_2 variations across the spectrum that MF did. This may, in part, be due to the effects of nuclear modulation (i.e. the $k_\pm$ terms in eq. (3) as well as overlap effects from the main peak with the $2\omega_-$ nuclear modulation terms).

In conclusion, we note that 2D-FT-ESR in the slow-motional and rigid limits is now a reality. We find that the variation of the nuclear modulation patterns, as well as their effects on the central ESR spectrum, are very sensitive to structure. Motional effects are clearly indicated via the T_2's of the central ESR spectrum and also by their effects on the deuteron modulation patterns. As techniques and analysis improve, SECSY-ESR should prove a very valuable tool in the study of structure and of slow motions.

Acknowledgement

This research was conducted using the Cornell National Supercomputer Facility.

References

[1] J. Gorcester and J.H. Freed, J. Chem. Phys. 85 (1986) 5375.
[2] J. Gorcester and J.H. Freed, J. Chem. Phys. 88 (1988) 4678.
[3] J. Gorcester and J.H. Freed, J. Magn. Reson. 78 (1988) 291.
[4] J. Gorcester, S. Rananavare and J.H. Freed, J. Chem. Phys. 90 (1989) 5764.
[5] J. Gorcester, G.L. Millhauser and J.H. Freed, in: Advanced EPR: Applications in biology and biochemistry, ed. A.J. Hoff (Elsevier, Amsterdam, 1989) ch. 5.
[6] J. Gorcester, G.L. Millhauser and J.H. Freed, in: Modern pulsed and continuous-wave electron spin resonance, eds. L. Kevan and M. Bowman (Wiley, New York, 1990) ch. 3.
[7] J.H. Freed, J. Chem. Soc. Faraday Trans., in press.
[8] M. Bowman, in: Modern pulsed and continuous-wave electron spin resonance, eds. L. Kevan and M. Bowman (Wiley, New York, 1990) ch. 1.
[9] G.L. Millhauser and J.H. Freed, J. Chem. Phys. 81 (1984) 37; 85 (1986) 63.
[10] L.J. Schwartz, G.L. Millhauser and J.H. Freed, Chem. Phys. Letters 127 (1986) 60.
[11] G.L. Millhauser, J. Gorcester and J.H. Freed, in: Electron magnetic resonance of the solid state, ed. J.A. Weil, Can. Chem. Soc. Publ. p. 71 (1987).
[12] L. Kevan and R.N. Schwartz, eds., Time domain electron spin resonance (Wiley, New York, 1979).
[13] L. Kevan and M.K. Bowman, eds., Modern pulsed and continuous-wave electron spin resonance (Wiley, New York, 1990).
[14] A. Hoff, ed., Advanced EPR: Applications in biology and biochemistry (Elsevier, Amsterdam, 1989).
[15] D. Gamliel and J.H. Freed, J. Magn. Reson. 89 (1990) 60.
[16] R.H. Crepeau, A. Dulcić, J. Gorcester, T.R. Saarinen and J.H. Freed, J. Mag. Reson. 84 (1989) 184.
[17] J. Lajzerowicz-Bonneteau, in: Spin labeling, theory and applications, ed. L.J. Berliner (Academic Press, New York, 1976).
[18] L.J. Schwartz, A.E. Stillman and J.H. Freed, J. Chem. Phys. 77 (1982) 5410.